International Journal of Multiphase Flow 49 (2013) 8–23

Contents lists available at SciVerse ScienceDirect

International Journal of Multiphase Flow

journal homepage: www.elsevier.com/locate/ijmulflow

Terminal velocities of clean and fully-contaminated drops in vertical pipes

Ryo Kurimoto *, Kosuke Hayashi, Akio Tomiyama

Graduate School of Engineering, Kobe University, 1-1, Rokkodai, Nada, Kobe, Japan

ARTICLE INFO

Article history:
Received 11 May 2012
Received in revised form 12 August 2012
Accepted 13 August 2012
Available online 24 August 2012

Keywords:
Drop
Drag force
Terminal velocity
Surfactant
Wall effect

ABSTRACT

Terminal velocities and shapes of drops rising through vertical pipes in clean and fully-contaminated systems are measured by using a high-speed video camera and an image processing method. Silicon oils and glycerol water solutions are used for the dispersed and continuous phases, respectively. Triton X-100 is used for surfactant. Clean and contaminated drops take either spherical, spheroidal or deformed spheroidal shapes when the diameter ratio λ is less than a critical value, λ_C, whereas they take bullet shapes for $\lambda > \lambda_C$ (Taylor drops). The applicability of available drag and Froude number correlations is examined through comparisons with the measured data. Effects of surfactant on the shape and terminal velocity of a Taylor drop are also discussed based on the experimental data and interface tracking simulations. The conclusions obtained are as follows: (1) drag and Froude number correlations proposed so far give reasonable estimations of the terminal velocities of clean drops at any λ, (2) the terminal velocities of contaminated drops are well evaluated by making the viscosity ratio μ^* infinity in the drag correlation for clean drops in the viscous force dominant regime, (3) the effects of surfactant on the shape and terminal velocity of a Taylor drop become significant as the Eötvös number, Eo_D, decreases and μ^* increases, and (4) the reduction in surface tension due to the addition of surfactant would be the cause of the increase in the terminal velocity and elongation of a contaminated Taylor drop.

1. Introduction

CMFD (Computational Multiphase Flow Dynamics) now plays an important role in designing various industrial systems. Among various CMFD methods, multi-fluid models and Euler–Lagrange methods are appropriate for dealing with a number of bubbles and drops in practical systems. These methods, however, require reliable closure relations for forces acting on fluid particles. Since the motion of a fluid particle is affected by the presence of surrounding walls, the wall effects must be taken into account in the closure relations when simulating fluid particles in conduits. Our knowledge on the wall effect is, however, still insufficient even for single fluid particles rising through stagnant liquids in vertical pipes.

The ratio, λ, of the sphere-volume equivalent diameter, d, of a fluid particle to the pipe diameter, D, is one of the important parameters in modeling the wall effect. The terminal velocity of a fluid particle depends on λ when λ is less than a certain critical value λ_C. The drag coefficient for $\lambda < \lambda_C$ has been represented as a product of the drag coefficient for a fluid particle in an infinite liquid and a wall effect multiplier. Haberman and Sayre (1958) theoretically derived a drag coefficient of a fluid particle in the viscous force dominant regime, which is a product of the Hadamard–Rybczynski solution for a fluid particle in infinite medium at low Reynolds numbers (Hadamard, 1911; Rybczynski, 1911) and a wall effect multiplier expressed in terms of λ and the viscosity ratio between the two phases. Hayashi and Tomiyama (2009) implemented an inertial effect multiplier to the Haberman's model to extend the model so as to be applicable to fluid particles at intermediate Reynolds numbers. Terminal velocity correlations for fluid particles rising through vertical pipes in the surface tension force and inertial force dominant regime were proposed by Clift et al. (1978), Wallis (1969) and Nakahara and Tomiyama (2003).

Bubbles take bullet shapes when $\lambda > \lambda_C$. They are called Taylor bubbles. The terminal velocity of a Taylor bubble is independent of λ, which means that the characteristic length governing the terminal velocity is not the bubble diameter but the pipe diameter. Many correlations for Taylor bubbles such as the ones by Dumitrescu (1943), Davies and Taylor (1950), Wallis (1969), Viana et al. (2003) and Hayashi et al. (2010) have been proposed. Since drops also take bullet shapes for $\lambda > \lambda_C$ and their terminal velocities are independent of λ, they can be also referred to as Taylor drops. Hayashi et al. (2011) have recently proposed a terminal velocity correlation for Taylor drops by carrying out a scaling analysis and interface tracking simulation. An appropriate combination of available drag and Froude number correlations may yield reasonable evaluations of the terminal velocities of fluid particles at any λ.

* Corresponding author. Tel./fax: +81 78 803 6304.
E-mail address: kurimoto@cfrg.scitec.kobe-u.ac.jp (R. Kurimoto).

0301-9322/$ - see front matter © 2012 Elsevier Ltd. All rights reserved.
http://dx.doi.org/10.1016/j.ijmultiphaseflow.2012.08.001

However the applicability of the drag correlations for $\lambda < \lambda_C$ has been examined only for $0 \leqslant \lambda \leqslant 0.6$. In addition, the critical diameter ratio depends on fluid properties and the pipe diameter, e.g., λ_C is about 0.6 for an air bubble rising through water in a pipe of 24.8 mm diameter (Nakahara and Tomiyama, 2003), whereas $\lambda_C \approx 1$ for fluid particles at low Reynolds numbers (Coutanceau and Texier, 1986; Almatroushi and Borhan, 2004). Hence the applicability of the correlations to a wide range of λ including $0.6 < \lambda < 1$ should be examined. This, in turn, requires experimental data of terminal velocity for a wide range of λ.

The above-mentioned correlations are applicable only to clean fluid particles. Multiphase systems are, however, often contaminated with surface-active agents. In spite of its practical importance, there are few studies on the wall effects on contaminated fluid particles in vertical pipes. Tomiyama et al. (2009) and Abe (2009) measured terminal velocities of contaminated Taylor bubbles at high Reynolds and high Eötvös numbers. They used three kinds of surfactants, i.e., Triton X-100, 1-pentanol and 1-octanol, and confirmed that these surfactants have no substantial effects on the terminal velocity of the Taylor bubble. Hayashi and Tomiyama (2012) investigated the effects of surfactant on the terminal velocities of low Morton number Taylor bubbles at various Eötvös numbers by making use of an interface tracking method. The simulation showed that the reduction of surface tension near the bubble nose due to the adsorption of surfactant is the cause of the increase in the terminal velocity of Taylor bubbles at low Eötvös numbers and the surfactant has substantially no effects on the terminal velocity at high Eötvös numbers since the bubble motion is independent of surface tension. Compared with the surfactant effects on Taylor bubbles, little is known on the effect of surfactant on Taylor drop shape and velocity. Almatroushi and Borhan (2004) carried out experiments on contaminated bubbles and drops in a vertical pipe and confirmed that surfactant decreases the terminal velocity of a fluid particle of $\lambda < \lambda_C$ due to the Marangoni effect (Levich, 1962) and surfactant increases the terminal velocity of a contaminated Taylor drop. They however dealt with only fluid particles at low Reynolds numbers.

In this study, terminal velocities of drops in vertical pipes in clean systems are measured for a wide range of λ to examine the applicability of the available drag and Froude number correlations. Fully-contaminated drops in pipes are also measured to examine the effects of surfactant on terminal velocity. In addition, surfactant effects on Taylor drop shape and velocity are investigated by making use of the interface tracking method proposed by Hayashi and Tomiyama (2012).

2. Review of drag and Froude number correlations

Let us briefly review drag and Froude number correlations for clean fluid particles in vertical pipes to make an appropriate combination of correlations for evaluating terminal velocity for a wide range of λ. The applicability of the selected correlations will be examined in Section 5. Surfactant effects on drag coefficients of fluid particles in pipes are discussed in Section 2.2.

2.1. Clean systems

The dynamics of a fluid particle rising through an infinite stagnant liquid is governed by the five forces, i.e., the viscous forces, $F_{\mu C}$ and $F_{\mu D}$, of the continuous and dispersed phases, the surface tension force F_σ, the inertial force F_i, and the buoyant force F_b (Tomiyama, 2004). The orders of these forces can be estimated by using the sphere-volume equivalent particle diameter, d, and the terminal velocity, V_{T0}, in an infinite stagnant liquid as the characteristic length and velocity scales, i.e., $F_{\mu C} \approx \mu_C V_{T0} d, F_{\mu D} \approx \mu_D V_{T0} d, F_\sigma \approx \sigma_0 d, F_i \approx \rho_C V_T^2 d^2$ and $F_b \approx \Delta\rho g d^3$, where μ is the viscosity, σ_0 the surface tension of clean interface, $\Delta\rho$ the difference of the density ρ between the continuous and dispersed phases, $\Delta\rho = \rho_C - \rho_D$, g the magnitude of the acceleration of gravity, and the subscripts C and D denote the continuous and dispersed phases (Tomiyama, 2004; Hayashi et al., 2010, 2011). Relevant dimensionless groups such as the Reynolds number, Re_0, of a free-rising fluid particle, the Eötvös number, Eo, and the viscosity ratio, μ^*, can be expressed in terms of these forces:

$$Re_0 = \frac{F_i}{F_{\mu C}} = \frac{\rho_C V_{T0} d}{\mu_C} \tag{1}$$

$$Eo = \frac{F_b}{F_\sigma} = \frac{\Delta\rho g d^2}{\sigma_0} \tag{2}$$

$$\mu^* = \frac{F_{\mu D}}{F_{\mu C}} = \frac{\mu_D}{\mu_C} \tag{3}$$

The density difference is considered in the gravitational effect by associating it with g, i.e., $\Delta\rho g$. Hence there is no need to introduce the density ratio, ρ_D/ρ_C (or $\Delta\rho/\rho_C$), as a dimensionless group (White and Beardmore, 1962). The drag coefficient, C_{D0}, of a fluid particle in an infinite stagnant liquid is given as a function of these dimensionless groups. Myint et al. (2006, 2008) recommended the following drag correlation for single drops in clean systems:

$$C_{D0} = \max[C_{D0}^{\mu}, C_{D0}^{\sigma i}] \tag{4}$$

where C_{D0}^{μ} and $C_{D0}^{\sigma i}$ are the drag coefficients in the viscous force dominant (μ) and the surface tension force and inertial force dominant (σ and i) regimes, respectively. The C_{D0}^{μ} is a combination of the Hadamard–Rybczynski solution for fluid particles in Stokes flows (Hadamard, 1911; Rybczynski, 1911) and the inertial effect multiplier K_{Is} (Schiller and Naumann, 1933):

$$C_{D0}^{\mu} = \frac{8}{Re_0}\left(\frac{2+3\mu^*}{1+\mu^*}\right)K_{Is} \tag{5}$$

$$K_{Is} = 1 + 0.15 Re_0^{0.687} \tag{6}$$

The drag coefficient, $C_{D0}^{\sigma i}$, is given by

$$C_{D0}^{\sigma i} = \frac{8}{3}\frac{Eo}{Eo+4} \tag{7}$$

which is based on a wave analogy (Mendelsen, 1967; Tomiyama et al., 1998). Eq. (4) implies that μ^* affects V_{T0} in the μ regime, whereas V_{T0} is independent of μ^* in the σ and i regime.

Joseph (2003) derived the following correlation for spherical cap bubbles, i.e. bubbles in the σ and i regime, using a viscous potential theory:

$$Fr = -\frac{8(1+8s)}{3N} + \frac{\sqrt{2}}{3}\left[1 - 2s - \frac{16s}{Eo} + \frac{32}{N^2}(1+8s)^2\right]^{1/2} \tag{8}$$

where s is the parameter representing the deviation of the interface from perfect sphericity near the nose and Fr and N are the Froude number and the inverse viscosity number defined by

$$Fr = \frac{V_{T0}}{\sqrt{\frac{\Delta\rho g d}{\rho_C}}} \tag{9}$$

$$N = \frac{\sqrt{\rho_C \Delta\rho g d^3}}{\mu_C} \tag{10}$$

Eq. (8) can be rearranged into a similar form to Eq. (7) by using the relation $C_D = 4/3Fr^2$.

Since the shape and terminal velocity, V_T, of a single fluid particle rising through a stagnant liquid in a vertical pipe depend on the ratio, λ (=d/D), of d to the pipe diameter D, the effects of λ must be implemented into drag correlations. When λ is less than a certain critical value λ_C, V_T depends on λ. Fluid particles in a pipe for $0 < \lambda < \lambda_C$ take either spherical, spheroidal or deformed spheroidal shape. In this case, the following drag correlation (Hayashi and Tomiyama, 2009) is of use:

$$C_D^{\mu} = \frac{8}{Re}\left(\frac{2+3\mu^*}{1+\mu^*}\right)[K_{Wh} + K_{ls} - 1] \tag{11}$$

where C_D^{μ} is the drag coefficient of a fluid particle rising through a vertical pipe in the μ regime, Re the Reynolds number of a fluid particle in the pipe, and K_{Wh} the wall effect multiplier (Haberman and Sayre, 1958), which are defined by

$$Re = \frac{\rho_C V_T d}{\mu_C} \tag{12}$$

$$K_{Wh} = \left(1 + c_0\lambda^5\frac{1-\mu^*}{2+3\mu^*}\right)\left(1 + c_1\frac{2+3\mu^*}{1+\mu^*}\lambda + c_2\frac{\mu^*}{1+\mu^*}\lambda^3 + c_3\frac{2-3\mu^*}{1+\mu^*}\lambda^5 + c_4\frac{1-\mu^*}{1+\mu^*}\lambda^6\right)^{-1} \tag{13}$$

where $c_0 = 2.2757$, $c_1 = -0.7017$, $c_2 = 0.20865$, $c_3 = 0.5689$ and $c_4 = -0.72603$. Hayashi and Tomiyama (2009) confirmed the validity of Eq. (8) for $0 \leqslant \lambda \leqslant 0.6$.

Clift et al. (1978) proposed the following correlation for bubbles and drops for $Re > 200$ and $Eo < 40$ by using experimental data in literature (Salami et al., 1965; Strom and Kintner, 1958; Uno and Kintner, 1956):

$$\frac{V_T}{V_{T0}} = (1-\lambda^2)^{3/2} \quad (0 \leqslant \lambda \leqslant 0.6) \tag{14}$$

The wall effect on the terminal velocity of a spherical-cap bubble in the i regime was investigated by Collins (1967) and Wallis (1969) proposed the following correlation based on Collins' data:

$$\frac{V_T}{V_{T0}} = 1.13e^{-\lambda} \quad (0.125 \leqslant \lambda \leqslant 0.6) \tag{15}$$

Many V_T correlations are available for Taylor bubbles. Among them, correlations proposed by Viana et al. (2003) and Hayashi et al. (2010) are the most reliable ones and applicable to a wide range of fluid properties. The latter correlation is given by

$$Fr_D = \sqrt{\frac{G\cdot H}{\frac{H}{0.35^2} + F}} \tag{16}$$

$$F = \frac{1}{Re_D}(1 - 0.05\sqrt{Re_D})$$

$$G = \left(1 + \frac{3.87}{Eo_D^{1.68}}\right)^{-18.4}$$

$$H = 0.0025[3 + G]$$

where Fr_D is the Froude number, Eo_D the Eötvös number and Re_D the Reynolds number defined by

$$Fr_D = \frac{V_T}{\sqrt{\Delta\rho g D/\rho_C}} \tag{17}$$

$$Eo_D = \frac{\Delta\rho g D^2}{\sigma_0} \tag{18}$$

$$Re_D = \frac{\rho_C V_T D}{\mu_C} \tag{19}$$

Hayashi et al. (2011) proposed a Fr_D correlation for Taylor drops by implementing the effects of the viscosity ratio into Eq. (16):

$$Fr_D = \sqrt{\frac{G\cdot H}{\frac{H}{0.35^2} + \left(\frac{1+1.9\mu^*}{1+0.31\mu^*}\right)F}} \tag{20}$$

which is also applicable to a wide range of fluid properties. Note that the coefficients in Eqs. (16) and (20) are changed from the original values in Hayashi et al. (2010, 2011). The reason of the change is given in Appendix A.1.

The applicability of the above-mentioned correlations for clean drops is summarized in Table 1. If Eq. (11) for drops in the μ regime is applicable to drops of $\lambda > 0.6$ and a drag model for drops in pipes in the σ and i regime is obtained, the drop rise velocity can be evaluated for a wide range of λ. Eq. (7) and the wall effect multiplier, Eq. (14), can be used for C_D of drops in the σ and i regime:

$$C_D^{\sigma i} = C_{D0}^{\sigma i} K_{Wc} = \frac{8}{3}\frac{Eo}{Eo+4}(1-\lambda^2)^{-3} \tag{21}$$

where K_{Wc} is the wall effect multiplier based on Eq. (14):

$$K_{Wc} = (1-\lambda^2)^{-3} \tag{22}$$

Therefore the drag correlation, C_{DS}, of drops is given by

$$C_{DS} = \max[C_D^{\mu}, C_D^{\sigma i}] \tag{23}$$

The force balance between the buoyancy and drag force for a drop is given by $\Delta\rho g\frac{\pi d^3}{6} = \frac{1}{2}C_D\rho_C V_T^2\frac{\pi d^2}{4}$. Re-arranging this using λ (=d/D) and Fr_D yields

$$C_{DT} = \frac{4}{3}\frac{\lambda}{Fr_D^2}, \tag{24}$$

The drag coefficient for single clean drops in a vertical pipe, which may be applicable to wide ranges of fluid properties and λ, is thus summarized as follows:

$$C_D = \begin{cases} \min[C_{DS}, C_{DT}] & \text{for } \lambda > 0.6 \\ C_{DS} & \text{otherwise} \end{cases} \tag{25}$$

2.2. Contaminated systems

Levich (1962) implemented the Marangoni effect into the Hadamard–Rybczynski solution for spherical drops in infinite medium:

Table 1
Available drag and Froude number correlations for small and Taylor drops.

System		Clean	
		Infinite	Pipe
Small drop	μ regime	Eq. (4): Myint et al., 2006, 2008 (combination of Eqs. (5) and (7)	Eq. (8): Hayashi and Tomiyama, 2009 (no validation for $\lambda > 0.6$)
	σ and i regime		None
Taylor drop	–	–	Eq. (20): Hayashi et al., 2011

$$C_{D0}^{\mu} = \frac{8}{Re_0}\left(\frac{2+3\mu^*+3C/\mu_C}{1+\mu^*+C/\mu_C}\right) \tag{26}$$

where C is a coefficient expressing the retardation of interface motion by surfactant. This equation was extended by Myint et al. (2006) so as to be applicable to non-spherical drops in the μ regime:

$$C_{D0}^{\mu} = \frac{8}{Re_0}\left(\frac{2+3\mu^*+3C/\mu_C}{1+\mu^*+C/\mu_C}\right)K_{Is} \tag{27}$$

They measured V_{T0} of fully-contaminated drops and confirmed that Eq. (27) with the limit $C \to \infty$:

$$C_{D0}^{\mu} = \frac{24}{Re_0}K_{Is}, \tag{28}$$

agrees well with the measured data. Eq. (28) is equivalent to the correlation for solid spheres (Schiller and Naumann, 1933), and therefore, the viscosity ratio does not affect V_{T0} of fully-contaminated drops even in the μ regime. Since we can take the limit $\mu^* \to \infty$ in Eq. (27) instead of $C \to \infty$ to obtain Eq. (28), drops of $\mu^* \to \infty$ can be also regarded as solid particles from the point of view of the drag coefficient.

The reduction in V_T at low λ is also caused by the Marangoni effect. Hence Eq. (11) may be also applicable to the fully-contaminated drops at low and intermediate Reynolds numbers by taking the limit $\mu^* \to \infty$, i.e.,

$$C_D^{\mu} = \frac{24}{Re}[K_{Wh}(\mu^* \to \infty, \lambda) + K_{Is} - 1] \tag{29}$$

where

$$K_{Wh}(\mu^* \to \infty, \lambda) = \frac{1-(c_0/3)\lambda^5}{1+3c_1\lambda+c_2\lambda^3-3c_3\lambda^5-c_4\lambda^6} \tag{30}$$

There are few Fr_D models for contaminated Taylor bubbles and Taylor drops in literature. A systematic database for effects of surfactant on Fr_D is indispensable to develop a Fr_D correlation for contaminated Taylor bubbles and Taylor drops.

3. Experimental method

The experimental apparatus is shown in Fig. 1. It consists of the vertical pipe, the lower and upper tanks. Two pipes of D = 11 and 21 mm were used. The pipe length was 1530 mm. The pipes and the tanks were made of transparent acrylic resin. Experiments were carried out at atmospheric pressure and room temperature. The temperature of the liquid and drops was kept at 298 ± 0.5 K.

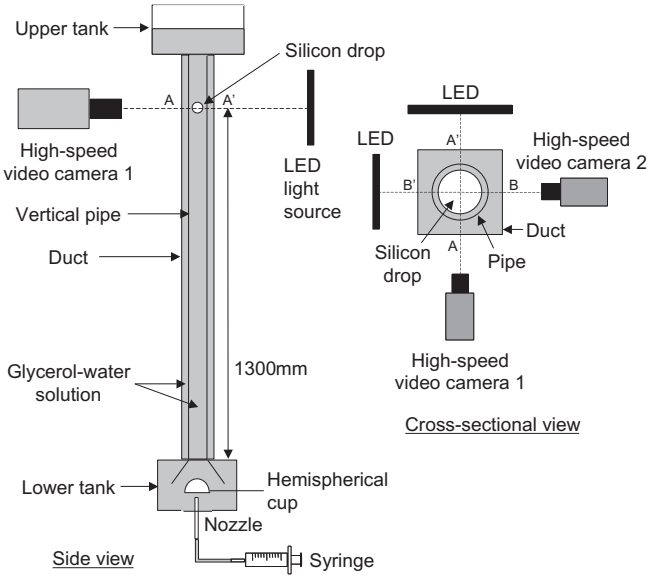

Fig. 1. Experimental apparatus.

Silicon oils of various viscosities (Sin-etsu Silicon, KF96-10, 30, 100, 300, and 500) and glycerol–water solutions were used for the dispersed and continuous phases, respectively. The glycerol–water solutions were made of water purified by using Elix-UV 10 (Millipore) and glycerol (Kishida Kagaku). The density, viscosity, surface tension and temperature were measured using a densimeter (Ando Keiki Co., Ltd., JIS B7525), a viscometer (Rion Co., Ltd., Viscotester VT-03E), capillary tubes (glass tube, 1.02 mm i.d.) and a digital thermometer (Sato Keiryoki MFG. Co., Ltd., SK-1250MC), respectively. Fluid properties were measured at least five times. Uncertainties estimated at 95% confidence in measured ρ, μ and σ were 0.021%, 0.53% and 4.0%, respectively. The measured values of ρ and μ agreed well with the data in literature (Ishikawa, 1968). The viscosity given in literature and the measured ρ and σ were used in calculations of the dimensionless numbers. Fluid systems examined are summarized in Table 2, in which M is the Morton number defined by

$$M = \frac{\mu_C^4 \Delta\rho g}{\rho_C^2 \sigma_0^3} \tag{31}$$

Two pipe diameters were used for most combination of dispersed and continuous liquid phases. Both clean and contaminated systems were examined for all the combinations of pipe diameters and liquids except Cases G, H and I. These exceptions were due to the instability shown in Fig. 3 and the breakup before reaching the measuring section. Cases A, B and C have almost the same Morton ($\log M \simeq -0.49$) and Eötvös numbers, whereas their viscosity ratios are different (μ^* = 0.11, 1.1 and 1.9). Therefore these cases were used to investigate the effects of μ^* on the drop shape and velocity. In each case, two values of Eo_D (Eo_D = 11 and 40) were tested to investigate its effects. Cases D, E and F and cases G, H and I were used for examining effects of Eo_D and μ^* in lower viscosity systems, i.e., $\log M \simeq -2.5$ in cases D, E and F and -4.7 in cases G, H and I. Triton X-100 ($C_8H_{17}C_6H_4(OCH_2CH_2)_{10}OH$) was used for surfactant. Measured surface tensions are plotted against the surfactant concentration in Fig. 2. The surface tension is almost constant when the concentration is larger than 1.0 mol/m^3, which indicates that the critical micelle concentration is at least lower than 1.0 mol/m^3. The concentration of 1.0 mol/m^3 was, therefore, used to carry out experiments on fully-contaminated drops. Since the surfactant concentration was less than 0.10 wt.%, the change in ρ_L and μ_L of the solution due to the presence of surfactant was negligible.

A clean glycerol–water solution was prepared by mixing the glycerol and water. The surfactant was then added to the solution and the solution was well re-mixed. The solution was stored in the upper and lower tanks and the pipe. The pure silicon oil was injected from the bottom of the lower tank and stored in the hemispherical glass cup. The stored oil was released as a single drop by rotating the cup. The silicone oil was not reused. Drop images were taken by using two high-speed video cameras (Integrated Design Tools Inc., Motionscope M3, frame rate = 10–400 frame/s, spatial resolution = 0.053–0.095 mm/pixel). These cameras were located at 1300 mm and 1100 mm above the bottom of the pipe as shown in Fig. 1 to examine whether or not the drop velocity reached the terminal velocity and the drop shape was axisymmetric. Several small drops did not move along the pipe axis. In addition, several Taylor drops did not take stable bullet shapes even at large λ due to some instability as shown in Fig. 3. This instability occurs at high Eo_D and low M in both clean and contaminated systems. The axisymmetry of drops was examined by comparing two drop images taken by the two high-speed video cameras. Only the axisymmetric drops rising rectilinearly along the pipe axis were

Table 2
Experimental conditions.

Case	Eo_D	D (mm)	log$M$	μ^*	ρ_C (kg/m^3)	ρ_D (kg/m^3)	μ_C (mPa s)	μ_D (mPa s)	σ_0 (mN/m)	Concentration of glycerol (wt.%)
A-a	41	21	−0.50	0.11	1240	955	262	29	30	93
A-b	11	11	−0.50	0.11	1240	955	262	29	30	93
B-a	40	21	−0.48	1.1	1240	970	262	291	29	93
B-b	11	11	−0.48	1.1	1240	970	262	291	29	93
C-a	40	21	−0.48	1.9	1240	970	262	485	29	93
C-b	11	11	−0.48	1.9	1240	970	262	485	29	93
D-a	36	21	−2.6	0.34	1219	955	85	29	32	85
D-b	9.8	11	−2.6	0.34	1219	955	85	29	32	85
E-a	35	21	−2.5	1.1	1219	965	85	97	31	85
E-b	9.7	11	−2.5	1.1	1219	965	85	97	31	85
F-a	36	21	−2.5	5.7	1219	970	85	485	30	85
F-b	9.8	11	−2.5	5.7	1219	970	85	485	30	85
G	33	21	−4.7	0.37	1189	935	25	9.4	33	74
H	31	21	−4.8	1.1	1189	955	25	29	33	74
I	31	21	−4.7	3.8	1189	965	25	97	31	74

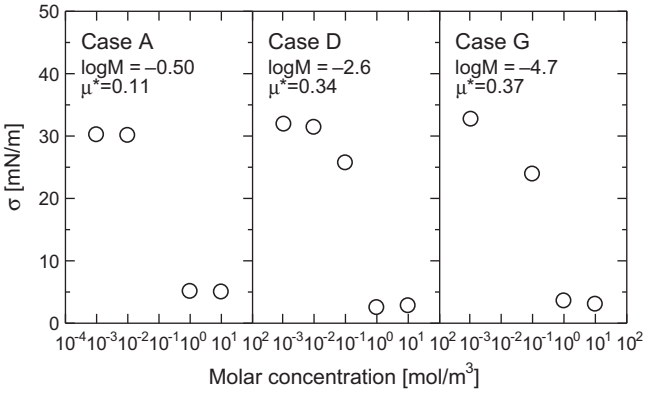

Fig. 2. Surface tension against surfactant concentration.

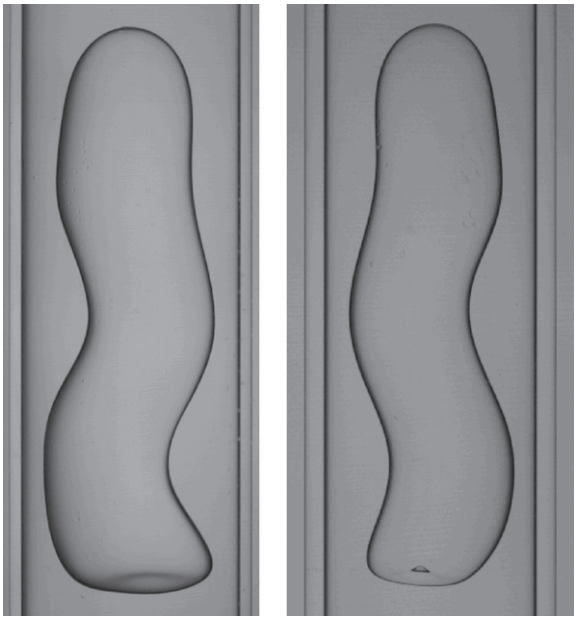

(a) Clean (Eo_D = 77) (b) Contaminated (Eo_D = 36)

Fig. 3. Clean and contaminated Taylor drops under unstable conditions (log$M$ = −2.5 and μ^* = 5.7).

used in this study. The pipe was enclosed with the acrylic duct. The gap between the pipe and the duct was filled with the same glycerol–water solution as that in the pipe to reduce optical distortion of drop images. LED light sources (Hayashi Watch-Works Co., Ltd., LP-2820) were used for back illumination.

The velocity, V_T, and the diameter, d, of a drop were calculated from the drop images using an image processing method (Tomiyama et al., 2002). An example of original drop images is shown in Fig. 4a. The drop image was transformed into binary images using an appropriate threshold level (Hosokawa and Tomiyama, 2003) as shown in Fig. 4b. Since drops were axisymmetric, all the horizontal cross-sections of a drop were circles of the radius R_i, where the index, i, denotes the pixel number in the vertical direction. The height of a circular disk in the image was one pixel and its physical length was Δz. The resultant circular disks were piled up in the vertical direction to reconstruct a three-dimensional drop shape as shown in Fig. 4c. Hence the sphere-volume equivalent diameter is given by $d = \sum_{i=1}^{N} (6R_i^2 \Delta z)^{1/3}$ where N is the total number of pixels in the vertical direction. The error in the number of pixels in binarization was estimated as ±0.5 pixel. The smallest drop diameter observed in this experiment was 1.3 mm. With the spatial resolution of 0.053 mm/pixel, the relative error in measured diameter is, therefore, less than ±2.1% for this drop. The error decreases with increasing d, e.g., 0.4% for a 12.9 mm drop in the 11 mm pipe. The drop terminal velocity was computed from the binary images by measuring the time required to rise 100 mm. The error in measured V_T due to the error in binarization was estimated as ±0.1%.

4. Interface tracking method

An interface tracking method proposed by Hayashi and Tomiyama (2012) was used in this study. The validity of the method has been confirmed through numerical simulations of clean and contaminated small bubbles and Taylor bubbles. The method is briefly described below.

The continuity and momentum equations for incompressible Newtonian fluid based on one-fluid formulation are given by

$$\nabla \cdot \boldsymbol{V} = 0 \tag{32}$$

$$\frac{\partial \boldsymbol{V}}{\partial t} + \boldsymbol{V} \cdot \nabla \boldsymbol{V} = -\frac{1}{\rho}\nabla P + \frac{1}{\rho}\nabla \cdot \mu[\nabla \boldsymbol{V} + (\nabla \boldsymbol{V})^T] + \boldsymbol{g} + \frac{1}{\rho}[\sigma\kappa \boldsymbol{n} + \nabla_S \sigma]\delta \tag{33}$$

where $\boldsymbol{V}$ is the velocity, t the time, $\boldsymbol{g}$ the acceleration of gravity, κ the curvature, $\boldsymbol{n}$ the unit normal to the interface, ∇_S (=$\nabla - \boldsymbol{nn}\cdot\nabla$) the surface gradient operator, δ the delta function, which is nonzero only at the interface, and the superscript T denotes the transpose. The term, $(\nabla_S\sigma)\delta$, is the tangential component of the surface

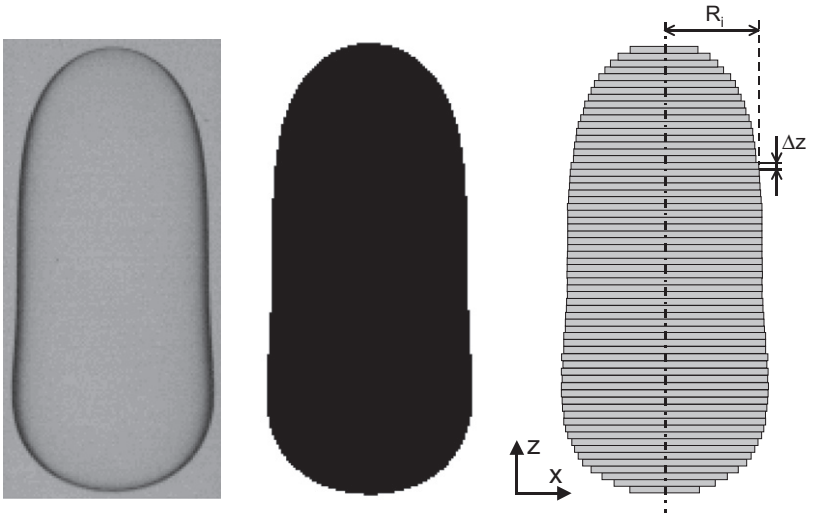

Fig. 4. Reconstruction of drop image.

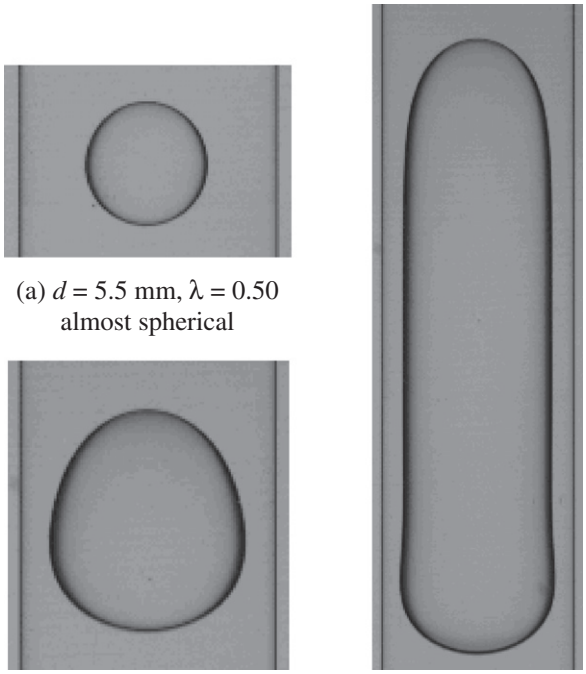

Fig. 5. Drops in case A-b ($D = 11$ mm).

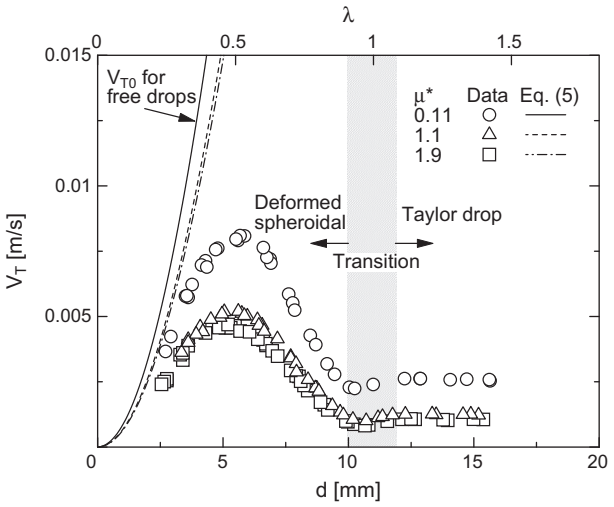

Fig. 6. Terminal velocities of clean drops in a high viscosity system (cases A-b, B-b and C-b: $\log M \simeq -0.49$, $Eo_D = 11$, $D = 11$ mm).

tension force causing the Marangoni effect. The continuity and momentum equations are solved using a projection method. A ghost fluid method (Kang et al., 2000) is utilized to deal with the normal component of the surface tension force in Eq. (33), whereas the tangential component is calculated using the continuum surface force model (Brackbill et al., 1992).

The interface is tracked by solving the following advection equation of the level set function ϕ (Sussman et al., 1994):

$$\frac{\partial \phi}{\partial t} + \boldsymbol{V} \cdot \nabla \phi = 0 \tag{34}$$

The re-initialization equation is also solved to maintain the property of ϕ as a distance function and the fluid volume is conserved using a correction method proposed by Meier (2000).

The transport equations of surfactant in the continuous phase and that at the interface are given by (Levich, 1962; Stone, 1990; Cuenot et al., 1997)

$$\frac{\partial C}{\partial t} + \boldsymbol{V} \cdot \nabla C = \nabla \cdot \alpha_C \nabla C \tag{35}$$

$$\frac{\partial \Gamma}{\partial t} + \nabla_S \cdot \Gamma \boldsymbol{V}_S = \nabla_S \cdot \alpha_S \nabla_S \Gamma + \dot{S}_\Gamma \tag{36}$$

where C is the surfactant concentration in the continuous phase, Γ the surfactant concentration at the interface, $\boldsymbol{V}_S$ the tangential component of $\boldsymbol{V}$, and α_C and α_S are the diffusion coefficient in the continuous phase and that at the interface, respectively. The source term $\dot{S}_\Gamma$ is the molar flux from the continuous phase to the interface due to the adsorption and desorption, i.e., $\dot{S}_\Gamma = -\alpha_C(\boldsymbol{n} \cdot \nabla C|_{int})$,

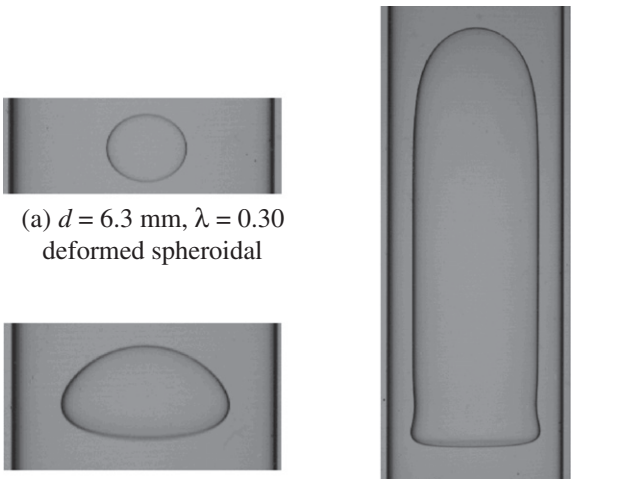

Fig. 7. Drops in case H (D = 21 mm).

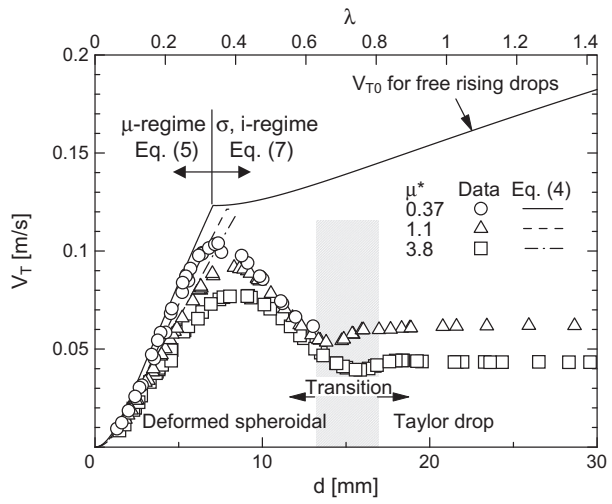

Fig. 8. Terminal velocities of clean drops in a low viscosity system (cases G, H and I: $\log M \simeq -4.7$, $Eo_D \simeq 32$, D = 21 mm).

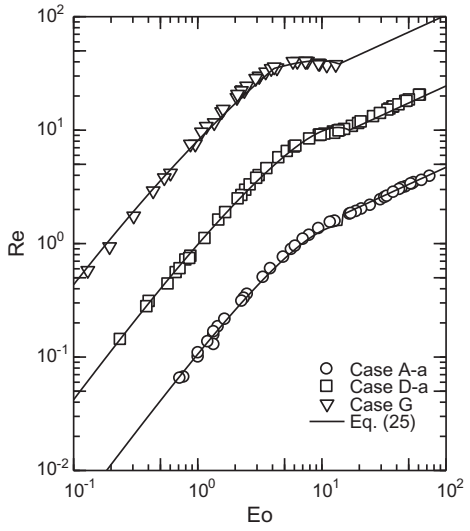

Fig. 9. Comparison between calculated and measured Re in low μ^* cases A-a, D-a and G.

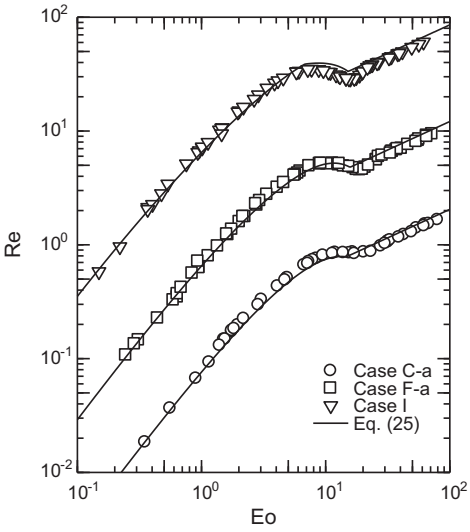

Fig. 10. Comparison between calculated and measured Re in high μ^* cases C-a, F-a and I.

which is evaluated by using the Frumkin–Levich model (Frumkin and Levich, 1947; Levich, 1962):

$$\dot{S}_\Gamma = k[C_S(\Gamma_{max} - \Gamma) - \beta\Gamma] \tag{37}$$

where k and β are parameters for the adsorption and desorption, respectively, Γ_{max} the saturation value of Γ and C_S the molar concentration of the continuous phase in the vicinity of the interface. Eqs. (35) and (36) are solved using the approximation method proposed by Muradoglu and Tryggvason (2008) and the extrapolation method proposed by Xu and Zhao (2003), respectively.

The surface tension is calculated by using

$$\sigma(\Gamma) = \max\left\{\sigma_0\left[1 + \eta\ln\left(1 - \frac{\Gamma}{\Gamma_{max}}\right)\right], \sigma_{CMC}\right\} \tag{38}$$

where η is the damping coefficient (Frumkin and Levich, 1947) and σ_{CMC} the surface tension at critical micelle concentration, e.g. σ_{CMC} = 2.5 mN/m at $\log M$ = −2.5 (see Fig. 2).

5. Results and discussion

5.1. Clean drops

5.1.1. Shape and terminal velocity

Fig. 5 shows examples of drop shapes in the pipe of D = 11 mm in case A-b ($\log M$ = −0.50, Eo_D = 11 and μ^* = 0.11). Drops for $\lambda < 0.5$ are almost spherical (Fig. 5a). Since the wall effect becomes significant with increasing λ, the fore-aft symmetry breaks at higher λ as shown in Fig. 5b. Fig. 5c shows an example of Taylor drops. As pointed out by Goldsmith and Mason (1962), the nose and rear of the Taylor drop in the high viscosity system are prolate spheroidal and oblate spheroidal, respectively.

Fig. 6 shows terminal velocities of drops for different viscosity ratios (μ^* = 0.34, 1.1 and 1.9 in cases A-b, B-b and C-b). The curves in the figure are the terminal velocities, V_{T0}, of drops in infinite stagnant liquids evaluated by using Eq. (5). The V_{T0} monotonously increases with d and decreases with increasing μ^*. In these cases, all the drops are in the μ regime. The presence of pipe wall

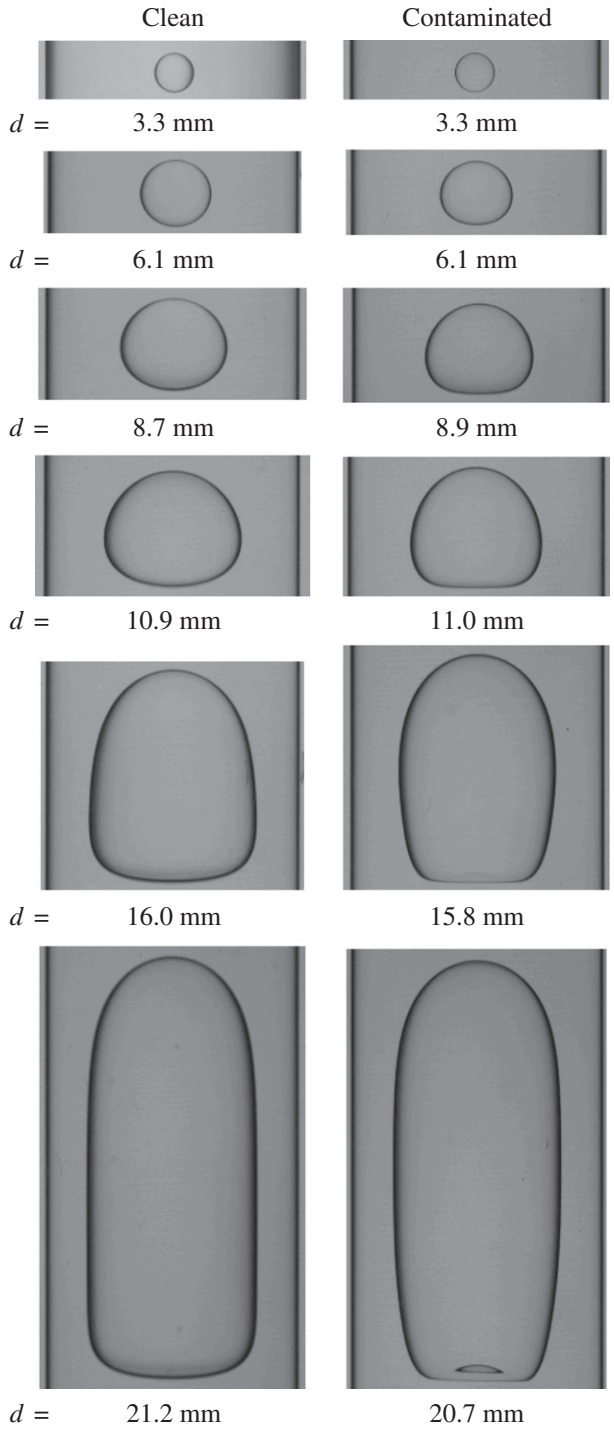

Fig. 11. Comparisons between clean and contaminated drop shapes in case D-a ($\log M = -2.6$, $Eo_D = 36$ and $\mu^* = 0.34$).

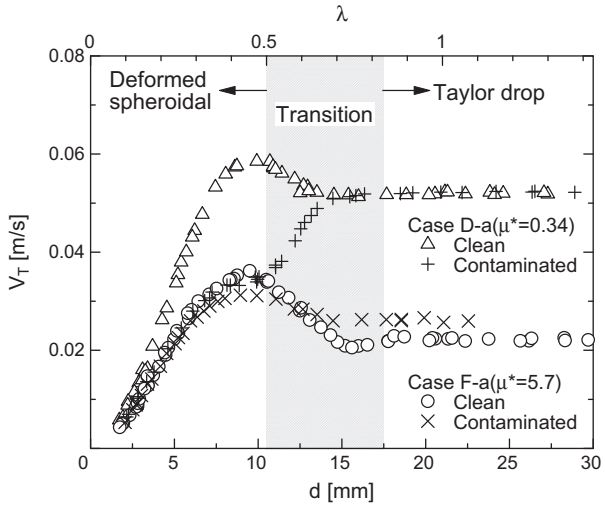

Fig. 12. Terminal velocities of clean and fully-contaminated drops in cases D-a and F-a ($\log M \simeq -2.5$ and $Eo_D = 36$).

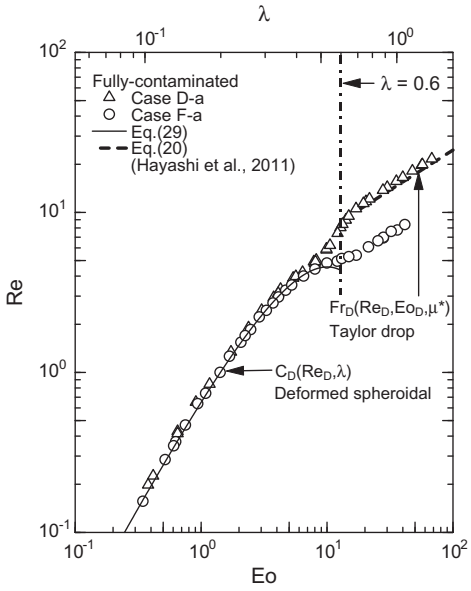

Fig. 13. Comparison between measured Reynolds numbers of drops in fully-contaminated systems in cases D-a and F-a and proposed correlation.

Table 3
Velocity ratio, $R_V = V_T$(contaminated)/V_T(clean).

Eo_D	Case A	Case B	Case C
(a) $\log M \simeq -0.49$			
	(μ^*=0.11)	(μ^*=1.1)	(μ^*=1.9)
11	1.14	1.30	1.39
40	1.01	1.07	1.06
Eo_D	Case D	Case E	Case F
(b) $\log M \simeq 2.5$			
	(μ^*=0.34)	(μ^*=1.1)	(μ^*=5.7)
9.8	1.24	1.59	2.59
36	1.01	1.08	1.17

decreases the terminal velocity, i.e., $V_T < V_{T0}$. The terminal velocity, V_T, depends on λ for $\lambda < 1$, whereas it is independent of λ for $\lambda > 1$. Hence the drops for $\lambda > 1$ are Taylor drops. There is a transition region from deformed spheroidal drops to Taylor drops.

Examples of drops in the pipe of $D = 21$ mm in the lowest μ_C case (case H: $\log M = -4.8$, $Eo_D = 31$ and $\mu^* = 1.1$) are shown in Fig. 7. The drops for $\lambda < \lambda_C$ are more deformed than those in Fig. 5a and b. The nose of the Taylor drop shown in Fig. 7c is spheroidal and the rear is flatter than that in Fig. 5c.

At $\log M \simeq -4.7$ (cases G, H and I), drops in infinite stagnant liquids transit from the μ regime to the σ and i regime at $d \approx 7$ mm as shown in Fig. 8. The tendency of V_T at $\log M \simeq -4.7$ is similar to that at $\log M \simeq -0.49$. However the effect of μ^* on V_T is very small in $0.5 < \lambda < 0.6$. Therefore the dominant force in this range is not the viscous force but the surface tension and inertial forces. The V_T of

Taylor drops, however, depends on μ^*, and therefore, the effects of μ^* on V_T reappear in the transition region.

5.1.2. Comparison between measured data and selected correlations

Fig. 9 shows comparisons between Eq. (25) and measured terminal velocities of low μ^* cases A-a, D-a and G. All the drops of $\lambda < \lambda_C$ in cases A and D are in the μ regime, whereas the drops for $5 \leqslant Eo \leqslant 10$ in case G are in the σ and i regime. The drops transit from deformed spheroids to bullet shapes in $10 < Eo < 20$. The selected correlations, Eq. (25), give reasonable evaluations of the terminal velocities of clean drops at any λ. The Reynolds numbers of drops with higher μ^*, i.e., $\mu^* \geqslant 1.9$, are plotted in Fig. 10. They are also reasonably evaluated by using Eq. (25). Comparisons between Eq. (25) and all the measured Re of clean drops are given in Appendix A.2.

5.2. Contaminated drops

5.2.1. Comparisons between clean and contaminated drops

Fig. 11 shows comparisons of drop shapes between clean and contaminated drops in case D-a. The surfactant clearly affects the drop shape. The difference between clean and contaminated Taylor drop shapes will be discussed later.

Terminal velocities of clean and fully-contaminated drops at $\log M \simeq -2.5$ (cases D-a and F-a) are compared in Fig. 12. The V_T of clean drops for $\lambda < \lambda_C$ depend on μ^*, and therefore, they are in the μ regime. The surfactant decreases V_T of the drops for $\lambda < 0.5$.

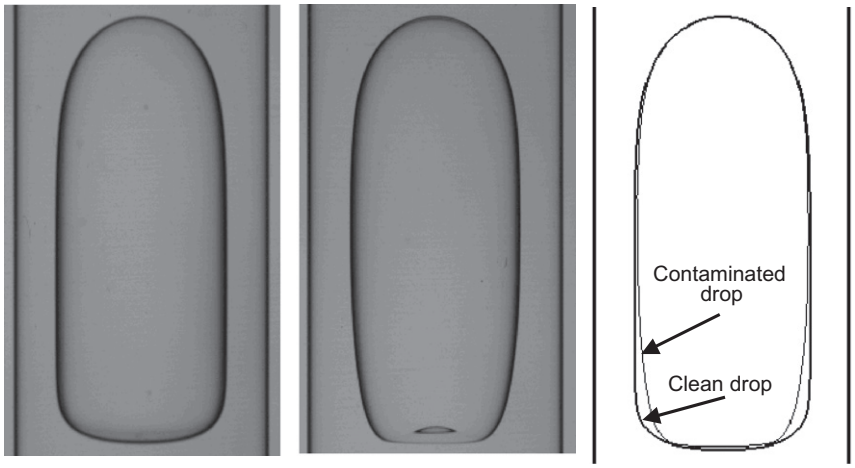

(a) clean $d = 21.2$ mm (b) contaminated $d = 20.7$ mm (c) outlines

Fig. 14. Comparison between clean and contaminated drop shapes (Case D-a: $\log M = -2.6$, $\mu^* = 0.34$, $Eo_D = 36$ and $R_V = 1.01$).

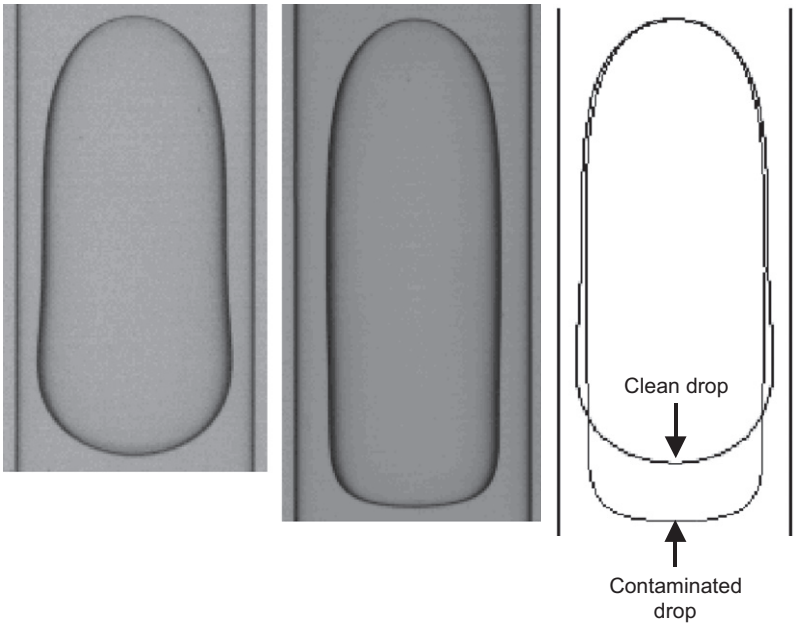

(a) clean $d = 12.8$ mm (b) contaminated $d = 13.0$ mm (c) outlines

Fig. 15. Comparison between clean and contaminated drop shapes (Case D-b: $\log M = -2.6$, $\mu^* = 0.34$, $Eo_D = 9.8$, and $R_V = 1.24$).

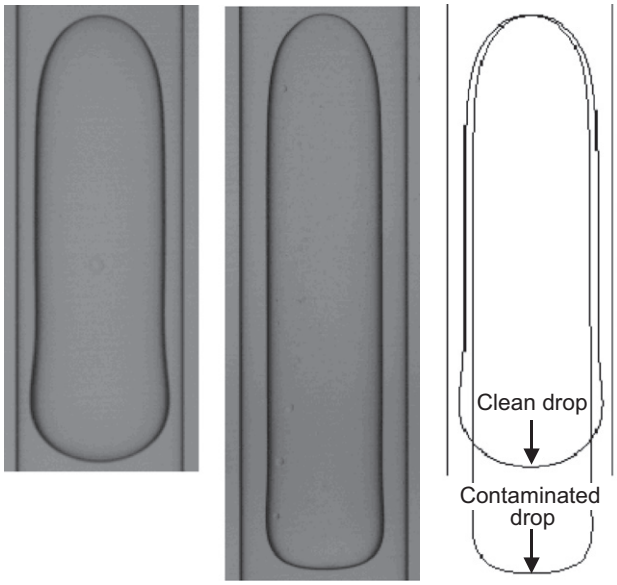

Fig. 16. Comparison between clean and contaminated drop shapes (Case F-b: $\log M = -2.5$, $\mu^* = 5.7$, $Eo_D = 9.8$ and $R_V = 2.59$).

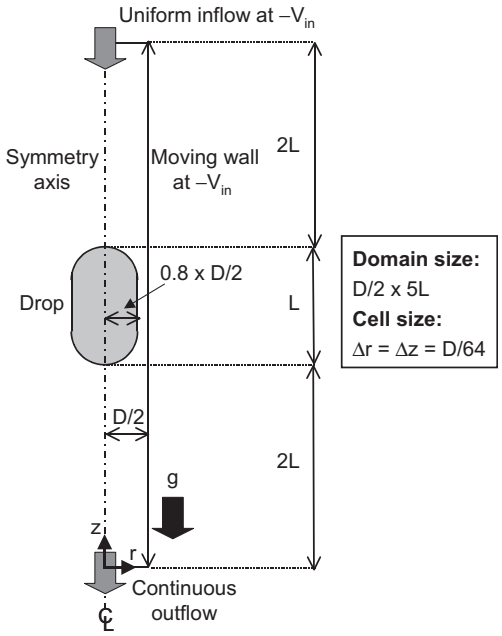

Fig. 17. Computational domain.

Table 4
Numerical conditions of M, μ^* and Eo_D.

	$\log M$	μ^*	Eo_D
Case D-a	−2.6	0.34	36
Case D-b	−2.6	0.34	9.8
Case F-b	−2.5	5.7	9.8

This is due to the Marangoni effect. The comparison of V_T between the contaminated drops in cases D-a and F-a indicates that μ^* does not have much influence on V_T when $\lambda < 0.5$ even though the drops are in the μ regime. Eq. (29) is compared with the data of cases D-a and F-a in Fig. 13. The data of these cases are collapsed in a single curve at small λ (λ is less than about 0.5) because the effect of μ^* on Re of small drops vanishes in the fully-contaminated systems. The correlation and data are in fair agreement up to $\lambda \simeq 0.5$.

There is only a slight difference in V_T between the clean and contaminated drops in case D-a, whereas the contaminated Taylor drops are 20% faster than the clean ones in case F-a. In contrast to the contaminated drops for $\lambda < 0.5$, the terminal velocity of contaminated Taylor drop depends on μ^*. Eq. (20) for clean Taylor drops can be used for the fully-contaminated drops in case D-a as shown in Fig. 13 since the surfactant does not have much influence on V_T in this particular case. The correlation, however, is not applicable to Case F-a because it does not take into account the surfactant effect. There are no correlations for evaluating Re in the region of transition from deformed spheroidal to Taylor drops in contaminated systems. Modeling the drop dynamics in the transition regime should be done in the future.

The ratio, R_V, of the terminal velocity of a fully-contaminated Taylor drop to that of a clean drop at the same values of the dimensionless numbers is summarized in Table 3. The ratio increases with μ^* and decreases with increasing Eo_D.

A comparison between clean and contaminated drop shapes in case D-a is shown in Fig. 14a and b. Fig. 14c shows the outlines of the drop shapes obtained using an edge detection method. The nose shapes are the same, whereas the rear of the contaminated drop is more slender than that of the clean drop. In addition, a dimple appears in the bottom of the contaminated drop. Fig. 15 shows a comparison of drop shapes at a lower Eo_D condition (case D-b). The contaminated drop is more slender than the clean drop not only in the rear region but also in the nose region. As shown in Fig. 16, the drop elongation is more marked at high μ^* (case F-b). This implies that a Taylor drop is more widely and densely covered with surfactant as μ^* increases and Eo_D decreases. To make detailed discussion on the surfactant distribution on drop surface, interface tracking simulations are carried out in the next section.

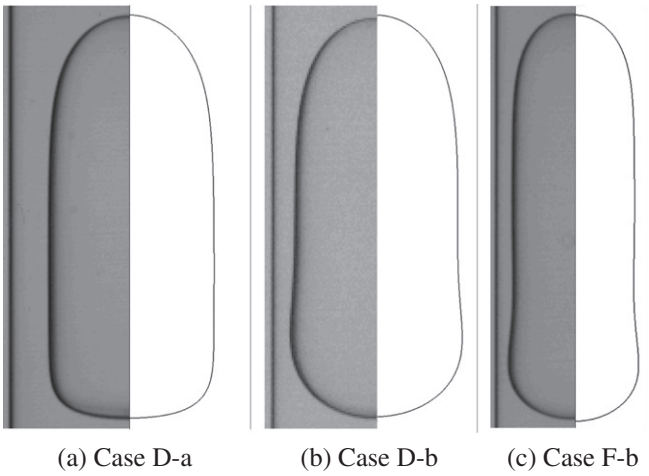

Fig. 18. Comparisons between measured (left) and predicted (right) clean drop shapes.

Table 5
Comparison of terminal velocities between measured and predicted clean drops.

	Measured V_T (m/s)	Predicted V_T (m/s)
Case D-a	0.052	0.0520
Case D-b	0.0046	0.00453
Case F-b	0.0016	0.00145

Table 6
Surfactant properties.

	β (mol/m^3)[a]	Γ_{max} (mol/m^2)[a]	k (m^3/mol s)	α_C, α_S (m^2/s)	η	La
Case D-a	1.18×10^{-5}	1.96×10^{-6}	5.0	7.0×10^{-4}	0.10	8.47×10^4
Case D-b	1.18×10^{-5}	1.96×10^{-6}	5.0	7.0×10^{-4}	0.10	8.47×10^4
Case F-b	1.18×10^{-5}	1.96×10^{-6}	130	1.0×10^{-5}	0.10	8.47×10^4

[a] Stebe et al. (1991).

The measured Froude numbers and shapes of Taylor drops are summarized in Appendix A.3. These data would be useful for validation of interface tracking methods.

5.2.2. Simulation of contaminated Taylor drops

Interface tracking simulations of contaminated Taylor drops were carried out to investigate the effects of surfactant on Taylor drops. Clean drops were first simulated for validation of the numerical method. Values of M, μ^* and Eo_D are summarized in Table 4. These are the same as those of the experimental conditions for the drops in Figs. 14–16. The drops of Figs. 14 and 15 (cases D-a and D-b) have the same M and μ^* but have different Eo_D, and those of Figs. 15 and 16 (case F-b) have the same M and Eo_D but have different μ^*. Two-dimensional cylindrical coordinates (r, z) were used. The computational domain is shown in Fig. 17. The left, top and bottom boundaries were the axis of symmetry, uniform inflow and continuous outflow, respectively. The right boundary moved downward at the inflow speed to simulate drops in stagnant liquid. The initial drop shape was a cylinder with two hemispheres. The dimensions of the domain were $D/2$ and $5L$ in the r and z directions, where L is the initial drop length. The computational cell was uniform and its width was $D/64$. The simulation for case D-a was also carried out with a 1.4 times longer domain and a two times higher spatial resolution. The difference in predicted terminal velocity due to the domain size and the spatial resolution was less than 0.78%. Predicted drop shapes and terminal velocities are compared with the measured data in Fig. 18 and in Table 5, respectively. Good agreements were obtained for both shape and velocity.

The surfactant properties, i.e., α_C, α_S, k, β, Γ_{max}, and η, are required for simulating contaminated drops. Databases of these physical properties, however, have not been established for the two-phase systems in this study. Hence the values of β and Γ_{max} for Triton X-100 in a liquid–liquid system similar to the present fluid systems, i.e., those in an oil–water system (Stebe et al., 1991) given in Table 6, were used. The bulk concentration, C_∞, was the same as that in the experiment, i.e., $C_\infty = 1.0$ mol/m^3. The Langmuir number, La, defined by

$$La = \frac{C_\infty}{\beta} \tag{39}$$

was, therefore, 8.5×10^4. The high La means that adsorption is more dominant than desorption. By referring the values of η used in front-tracking simulations of a water drop falling in silicon oil carried out by Yamamoto et al. (2008), η was set at 0.10. They investigated the effects of the surface Schmidt number, Sc_S ($=\mu_C/\rho_C\alpha_S$), on the drop motion and obtained a good agreement in velocity field between the prediction and measurement by setting the order of Sc_S $10^0 \sim 10^1$. It is therefore assumed that the order of Sc_S in the present two-phase system is similar to those used in their simulations, i.e. $Sc_S = 0.1$, 0.1 and 7 in Cases D-a, D-b and F-b, resulting in $\alpha_S = 7.0 \times 10^{-4}$, 7.0×10^{-4} and 1.0×10^{-5} in Cases D-a, D-b and F-b, respectively. The bulk diffusion coefficient, α_C, was assumed to be the same as α_S: $\alpha_C = \alpha_S$ (Cuenot et al., 1997; Takagi et al., 2009). The value of k was determined by trial and error so as to reproduce the measured drop length.

Predicted shapes and terminal velocities of the contaminated drops are compared with the measured data in Fig. 19 and Table 7,

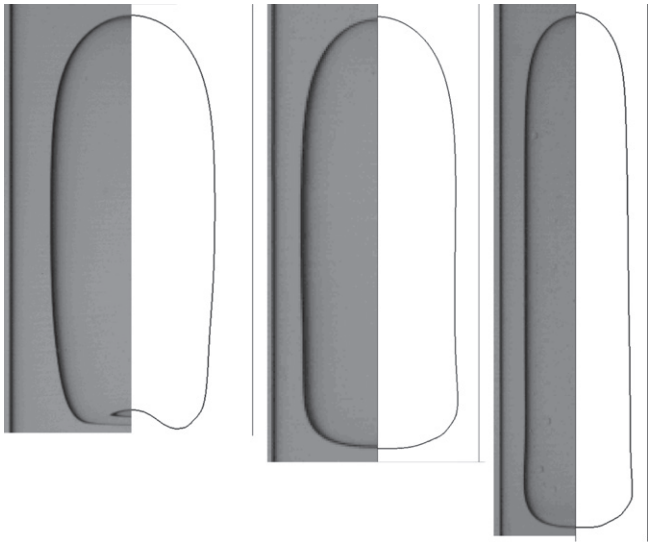

Fig. 19. Comparisons between measured (left) and predicted (right) contaminated drop shapes.

Table 7
Comparison of terminal velocities between measured and predicted contaminated drops.

	Measured V_T (m/s)	Predicted V_T (m/s)
Case D-a	0.052	0.0515
Case D-b	0.0057	0.00565
Case F-b	0.0042	0.00415

respectively. The predictions and the measured data are in good agreement, which allows us at least to qualitatively discuss main causes of the drop elongation and the increase in velocity. Relevant dimensionless groups for the drop dynamics in the presence of surfactant were calculated using the values of V_T as shown in Table 8. The dimensionless groups, Pe, Pe_S and Ha, are the Peclet number, the interfacial Peclet number and the Hatta number, respectively. They are defined by

$$Pe = \frac{V_T D}{\alpha_C} \tag{40}$$

$$Pe_S = \frac{V_T D}{\alpha_S} \tag{41}$$

Table 8
Dimensionless groups concerning with dynamics of contaminated drop.

	Re_D	Pe	Pe_S	Ha
Case D-a	16	1.5	1.5	2.0
Case D-b	0.89	0.089	0.089	9.74
Case F-b	0.65	4.6	4.6	345

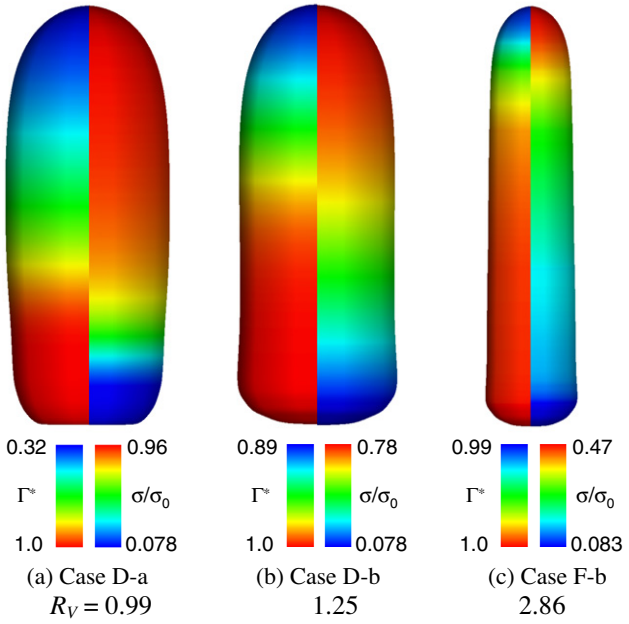

(a) Case D-a $R_V = 0.99$ (b) Case D-b 1.25 (c) Case F-b 2.86

Fig. 20. Distribution of Γ/Γ_{max} and σ/σ_0.

$$Ha = \frac{kC_\infty D}{V_T} \tag{42}$$

The Hatta number is the ratio of the adsorption velocity to the bubble rising velocity. The adsorption was faster than the bubble velocity in all the cases. Especially, in case F-b, the adsorption was much more dominant than the advection. Because of high Pe and Pe_S, the advection was also faster than the diffusion both in the continuous phase and at the interface in case F-b.

Fig. 20 shows the distributions of the dimensionless surface concentration Γ^* ($=\Gamma/\Gamma_{max}$) and the surface tension scaled by σ_0. The whole drop surfaces are covered with surfactant due to fast adsorption. The drop noses take the lowest values of Γ^*, and the rears are fully packed with surfactant. The surface tensions in the bottom regions for the three cases are not so different. On the other hand, Γ^* at the noses take different values, i.e., $\sigma/\sigma_0 = 0.96$, 0.78 and 0.47 in cases D-a, D-b and F-b, respectively. The reduction of σ in the nose region is small in case D-a. In this case, R_V is almost unity and the nose shape is not affected by the presence of surfactant. To the contrary, in case F, the drastic σ reduction takes place in the nose region, R_V is high and the drop is much elongated. The trends of R_V and shape in case D-b are in-between. Hence the reduction of σ would be the cause of drop elongation and the reduction in the nose region increases V_T.

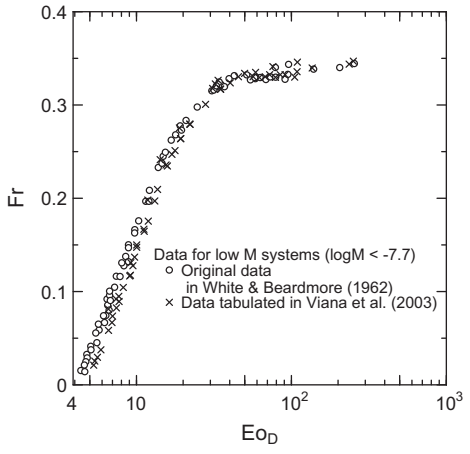

Fig. A1. Froude numbers of Taylor bubbles in low Morton number systems (White and Beardmore, 1962).

6. Conclusions

Terminal velocities and shapes of clean and fully-contaminated drops in vertical pipes were measured to examine the applicability of available correlations of drag coefficient and Froude number. Experimental conditions for clean drops were $-0.48 < \log M < -4.8$, $9.7 < Eo_D < 41$ and $0.11 < \mu^* < 5.7$, where M is the Morton number, Eo_D the Eötvös number and μ^* the viscosity ratio. Drops took either spherical, spheroidal or deformed spheroidal shapes when the diameter ratio, λ, of the bubble diameter to the pipe diameter was less than a critical value, λ_C, whereas they took bullet shapes, i.e., Taylor drop shapes, for $\lambda > \lambda_C$. Experiments on contaminated drops were carried out for $-0.48 < \log M < -2.6$, $9.7 < Eo_D < 41$ and $0.11 < \mu^* < 5.7$, to investigate effects of surfactant on V_T and the shape. The surfactant effects on Taylor drops were also discussed by making use of an interface tracking method. The conclusions obtained are as follows:

(1) The combination of available drag and Froude number correlations, Eq. (25), gives reasonable estimations of the terminal velocities of clean drops for a wide range of λ.
(2) The terminal velocities of contaminated drops are well evaluated by taking the limit $\mu^* \to \infty$ in the drag correlation of Hayashi and Tomiyama (2009).
(3) The effects of surfactant on the shape and terminal velocity of a Taylor drop become significant as Eo_D decreases and μ^* increases.
(4) The reduction in surface tension due to the adsorption of surfactant would cause the increase in the terminal velocity and the elongation of a Taylor drop.

Acknowledgements

This work has been supported by the Japan Society for the Promotion of Science (grant-in-aid for scientific research (B), No. 24360070).

Appendix A

A.1. Froude number correlations for Taylor bubbles and drops

The coefficients in the Froude number correlation for Taylor bubbles, Eq. (16), slightly differ from those in the original correlation proposed by Hayashi et al. (2010). The original correlation is given by

$$Fr_D = \sqrt{\frac{0.0089\left(1+\frac{41}{Eo_D^{1.96}}\right)^{-4.63}}{0.0725+\frac{(1-0.11Re_D^{0.33})}{Re_D}}} \tag{A.1}$$

The reason of this modification is as follows. White & Beardmore's experimental data of Fr (1962) tabulated by Viana et al. (2003) were used to determine the values of coefficients in Eq. (A.1). The authors, however, noticed that the tabulated data for Taylor bubbles in low Morton number systems involve large errors and differ from the original data in White and Beardmore (1962). The difference is shown in Fig. A1. Hence the coefficients in Eq. (A.1) were re-determined using the original data. Fig. A2 shows a comparison between

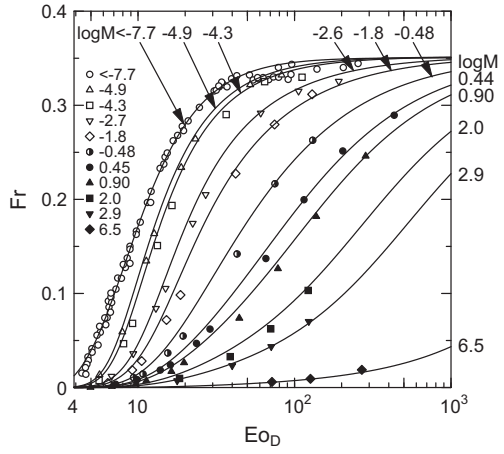

Fig. A2. Comparisons of Froude number between Eq. (16) and White and Beardmore's experimental data.

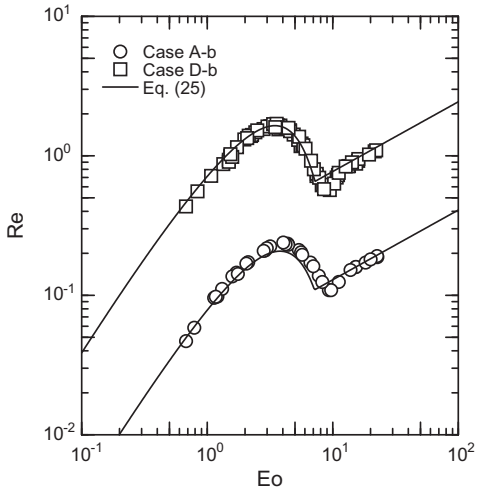

Fig. A5. Comparison between calculated and measured *Re* in cases A-b and D-b.

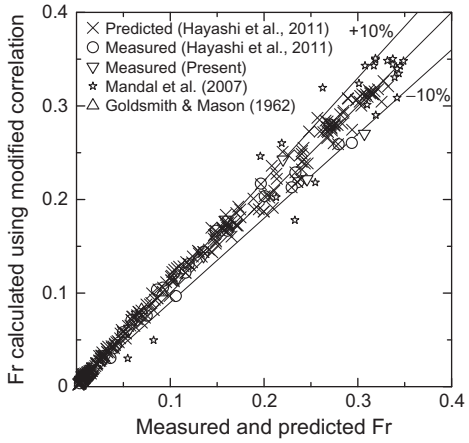

Fig. A3. Comparisons between Froude numbers calculated using Eq. (20) and the data given in Hayashi et al. (2011).

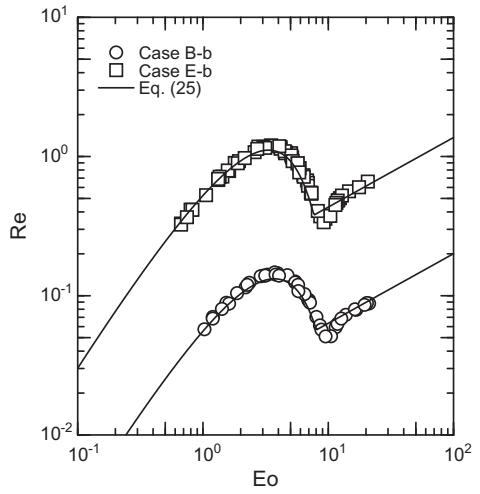

Fig. A6. Comparison between calculated and measured *Re* in cases B-b and E-b.

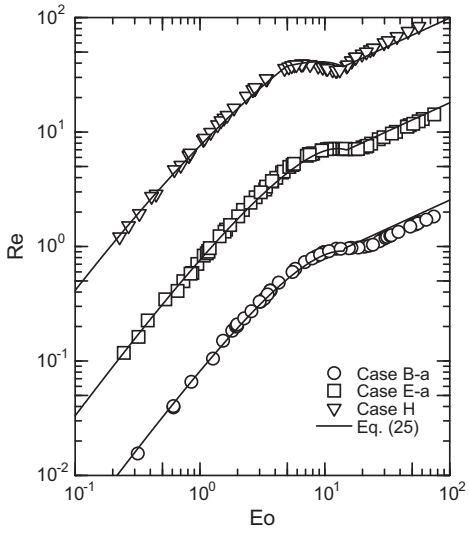

Fig. A4. Comparison between calculated and measured *Re* in cases B-a, E-a and H.

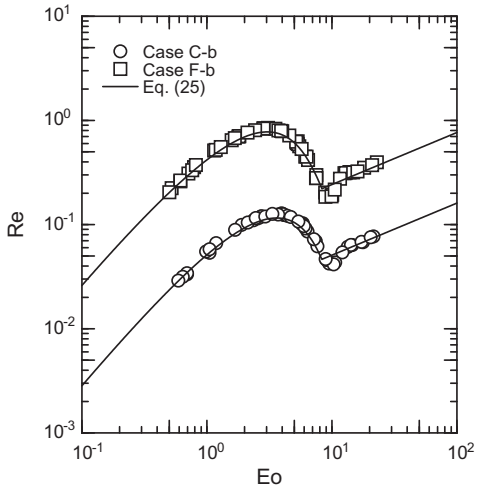

Fig. A7. Comparison between calculated and measured *Re* in cases C-b and F-b.

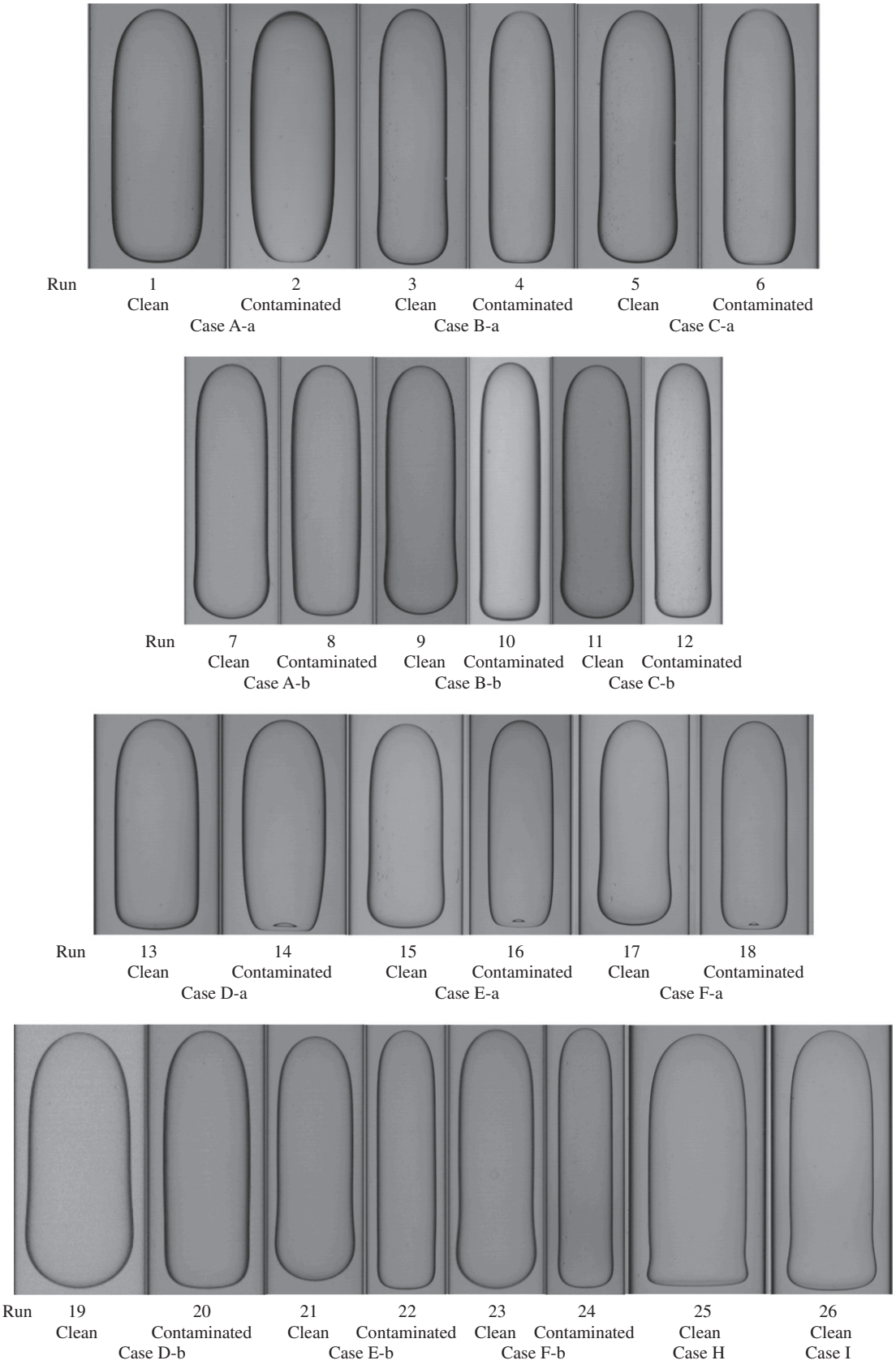

Fig. A8. Taylor drop shapes.

Eq. (16) and the data for Taylor bubbles. Good agreements are obtained for various values of Eo_D and M. Since the correlation for Taylor drops is an extension of Eq. (A.1), the correlation for Taylor drops proposed by Hayashi et al. (2011) was also modified to Eq. (20). Comparisons of Fr between Eq. (20) and the measured and numerical data are shown in Fig. A3.

Table A1
Dimensionless numbers of Taylor drops.

Run	Case	System	Fr_D	$\log M$	Eo_D	μ^*	λ	ρ_C (kg/m^3)	ρ_D (kg/m^3)	μ_C (mPa s)	μ_D (mPa s)	σ_0 (mN/m)	D (mm)
1	A-a	Clean	0.14	−0.50	41	0.11	1.02	1240	955	262	29	30	21
2		Contaminated	0.14	−0.50	41	0.11	1.02	1240	955	262	29	30	21
3	B-a	Clean	0.0065	−0.48	40	1.1	1.09	1240	970	262	291	29	21
4		Contaminated	0.0069	−0.48	40	1.1	1.09	1240	970	262	291	29	21
5	C-a	Clean	0.057	−0.48	40	1.9	1.03	1240	970	262	485	29	21
6		Contaminated	0.060	−0.48	40	1.9	1.05	1240	970	262	485	29	21
7	A-b	Clean	0.016	−0.50	11	0.11	1.34	1240	955	262	29	30	11
8		Contaminated	0.019	−0.50	11	0.11	1.31	1240	955	262	29	30	11
9	B-b	Clean	0.0082	−0.48	11	1.1	1.35	1240	970	262	291	29	11
10		Contaminated	0.011	−0.48	11	1.1	1.34	1240	970	262	291	29	11
11	C-b	Clean	0.0070	−0.48	11	1.9	1.36	1240	970	262	485	29	11
12		Contaminated	0.0098	−0.48	11	1.9	1.35	1240	970	262	485	29	11
13	D-a	Clean	0.25	−2.6	36	0.34	1.01	1219	955	85	29	32	21
14		Contaminated	0.25	−2.6	36	0.34	0.99	1219	955	85	29	32	21
15	E-a	Clean	0.075	−2.5	35	1.1	1.02	1219	965	85	97	31	21
16		Contaminated	0.081	−2.5	35	1.1	1.05	1219	965	85	97	31	21
17	F-a	Clean	0.064	−2.5	36	5.7	1.02	1219	970	85	485	30	21
18		Contaminated	0.074	−2.5	36	5.7	1.00	1219	970	85	485	30	21
19	D-b	Clean	0.030	−2.6	9.8	0.34	1.16	1219	955	85	29	32	11
20		Contaminated	0.037	−2.6	9.8	0.34	1.18	1219	955	85	29	32	11
21	E-b	Clean	0.0090	−2.5	9.7	1.1	1.34	1219	965	85	97	31	11
22		Contaminated	0.014	−2.5	9.7	1.1	1.38	1219	965	85	97	31	11
23	F-b	Clean	0.011	−2.5	9.8	5.7	1.33	1219	970	85	485	30	11
24		Contaminated	0.021	−2.5	9.8	5.7	1.36	1219	970	85	485	30	11
25	H	Clean	0.30	−4.8	31	1.1	1.11	1189	955	25	29	33	21
26	I	Clean	0.22	−4.7	31	3.8	1.16	1189	965	25	97	31	21

A.2. Comparison between calculated and measured Re

Measured Reynolds numbers of clean drops in vertical pipes are given in Figs. A4–A7. The correlation, Eq. (25), is also drawn in the figures for comparison. See Figs. 9 and 10 for cases A-a, D-a, C-a, F-a, G and I.

A.3. Shapes and Froude numbers of Taylor drops

Shapes and Froude numbers of clean and contaminated Taylor drops are summarized in Fig. A8 and Table A1, respectively. Since the clean Taylor drops in case G and contaminated Taylor drops in cases G, H and I showed unstable motion and non-axisymmetric shapes, they were omitted.

References

Abe, S., 2009. Mass Transfer between Gas and Liquid in Carbon Dioxide–Water Bubbly Flows in Vertical Pipe. Ph.D. Thesis, Kobe University (in Japanese).

Almatroushi, E., Borhan, A., 2004. Surfactant effect on the buoyancy-driven motion of bubbles and drops in a tube. Annals of the New York Academy of Sciences 1027, 330–341.

Brackbill, J.U., Kothe, D.B., Zemach, C., 1992. A continuum method for modeling surface tension. Journal of Computational Physics 100, 335–354.

Clift, R., Grace, J.R., Weber, M.E., 1978. Bubbles, Drops, and Particles. Academic Press, New York.

Collins, R., 1967. The effect of a containing cylindrical boundary on the velocity of a large gas bubble in a liquid. Journal of Fluid Mechanics 28, 97–112.

Coutanceau, M., Texier, A., 1986. Experimental investigation of the creeping motion of a drop in a vertical tube. Experiments in Fluid 4, 241–246.

Cuenot, B., Magnaudet, J., Spennato, B., 1997. The effects of slightly soluble surfactants on the flow around a spherical bubble. Journal of Fluid Mechanics 339, 25–53.

Davies, R.M., Taylor, G.I., 1950. The mechanics of large bubbles rising through liquids in tubes. Proceedings of the Royal Society of London A200, 375–390.

Dumitrescu, D.T., 1943. Stromung and Einer Luftbluse in Senkrechten rohr. Zeitschrift für Angewandte Mathematik und Mechanik 23, 139–149.

Frumkin, A., Levich, V.G., 1947. On surfactants and interfacial motion. Zhurnal Fizicheskoi Khimii 21, 1183–1204 (in Russian).

Goldsmith, H.L., Mason, S.G., 1962. The movement of single large bubbles in closed vertical tubes. Journal of Fluid Mechanics 10, 42–58.

Haberman, W.L., Sayre, R.M., 1958. Motion of Rigid and Fluid Spheres in Stationary and Moving Liquids Inside Cylindrical Tubes. David Taylor Model Basin Report, No. 1143.

Hadamard, J.S., 1911. Mouvement permanent tent d'une sphere liquide et visquese dans un liquide visqueux. Comptes Rendus de l'Academie des Science 152, 1735–1738.

Hayashi, K., Tomiyama, A., 2009. A drag correlation of fluid particles rising through stagnant liquids in vertical pipes at intermediate Reynolds numbers. Chemical Engineering Science 64, 3019–3028.

Hayashi, K., Kurimoto, R., Tomiyama, A., 2010. Dimensional analysis of terminal velocity of Taylor bubble in a vertical pipe. Multiphase Science and Technology 22, 197–210.

Hayashi, K., Kurimoto, R., Tomiyama, A., 2011. Terminal velocity of a Taylor drop in a vertical pipe. International Journal of Multiphase Flow 37, 241–251.

Hayashi, K., Tomiyama, A., 2012. Effects of surfactant on terminal velocity of a Taylor bubble in a vertical pipe. International Journal of Multiphase Flow 39, 78–87.

Hosokawa, S., Tomiyama, A., 2003. Lateral force acting on a deformed single bubble due to presence of wall. Transaction of Japanese Society of Mechanical Engineers, Series B 69 (686), 2214–2220 (in Japanese).

Ishikawa, T., 1968. Kongou Ekinendo No Riron. Maruzen (in Japanese).

Joseph, D., 2003. Rise velocity of a cap bubble. Journal of Fluid Mechanics 488, 213–223.

Kang, M., Fedkiw, R.P., Liu, X.-D., 2000. A boundary condition capturing method for multiphase incompressible flow. Journal of Scientific Computing 15 (3), 323–360.

Levich, V.G., 1962. Physicochemical Hydrodynamics. Prentice-Hall.

Meier, M., 2000. Towards a DNS of multiphase flow. Technical report No. LKT-01-00. Laboratorium fur Kerntechnik Institutfu furEnergietechnik, ETH Zurich.

Mendelsen, H.D., 1967. The prediction of bubble terminal velocities from wave theory. AIChE Journal 13, 250–253.

Muradoglu, M., Tryggvason, G., 2008. A front-tracking method for computation on interfacial flows with soluble surfactants. Journal of Computational Physics 227, 2238–2262.

Nakahara, Y., Tomiyama, A., 2003. Shapes and rising velocities of single bubbles in vertical pipes. Transaction of the Japanese Society of Mechanical Engineers, Series B 69 (685), 2002–2009 (in Japanese).

Rybczynski, W., 1911. On the translatory of a fluid sphere in a viscous medium. Bulletin of the Academy of Sciences, Cracow, Series A, 40–46.

Salami, E., Vignes, A., Le Goff, P., 1965. Hydrodynamique des dispersions. II. Effet de paroi. Mouvement d'une goutte ou d'une bulle dans un fluide immobile contenu dans un tube vertical de petit diametre. Genie Chimique 94, 67–77.

Schiller, L., Naumann, A., 1933. Uber die grundlegende berechunung bei der schwekraft-aufbereitung. Zeitschrift des Vereines Deutscher Ingenieure 44, 318–320.

Stone, H.A., 1990. A simple derivation of the time-dependent convective-diffusion equation for surfactant transport along a deforming interface. Physics of Fluids A 2 (1), 111–112.

Stebe, K.J., Lin, S., Maldarelli, C., 1991. Remobilizing surfactant retarded fluid interface. I. Stress-free conditions at the interfaces of micellar solutions of surfactants with fast sorption kinetics. Physics Fluids A 3, 3–20.

Strom, J.R., Kintner, R.C., 1958. Wall effect for the fall of single drops in stagnant liquids. AIChE Journal 4, 153–156.

Sussman, M., Smereka, P., Osher, S., 1994. A level set approach for computing solutions to incompressible two-phase flow. Journal of Computational Physics 114 (1), 146–159.

Takagi, S., Ogasawara, T., Fukuta, M., Matsumoto, Y., 2009. Surfactant effect on the bubble motions and bubbly flow structures in a vertical channel. Fluid Dynamics Research 41, 065003.

Tomiyama, A., Kataoka, I., Zun, I., Sakaguchi, T., 1998. Drag coefficients of single bubbles under normal and micro gravity conditions. JSME International Journal, Series B 41, 472–479.

Tomiyama, A., Celata, G.P., Hosokawa, S., Yoshida, S., 2002. Terminal velocity of single bubbles in surface tension force dominant regime. International Journal of Multiphase Flow 28, 1497–1519.

Tomiyama, A., 2004. Drag, lift and virtual mass forces acting on a single bubble. In: Proceedings of the 3rd International Symposium on Two-Phase Flow Modeling and Experimentation, CD-ROM, Pisa, Italy, 10 pages.

Tomiyama, A., Abe, S., Hayashi, K., Hosokawa, S., 2009, Dissolution of carbon dioxide bubbles in clean and contaminated systems. In: Proceedings of the 5th European-Japanese Two-Phase Flow Group Meeting, Spolete, Italy, 9 p.

Uno, S., Kintner, R.C., 1956. Effect of wall proximity on the rate of rise of single air bubbles in a quiescent liquid. AIChE Journal 2, 420–425.

Viana, F., Pardo, R., Yanez, R., Trallero, J.L., Joseph, D., 2003. Universal correlation for the rise velocity of long gas bubbles in round pipes. Journal of Fluid Mechanics 494, 79–398.

Wallis, D.B., 1969. One-dimensional Two-phase Flow. McGraw-Hill, New York.

Myint, Win, Hosokawa, S., Tomiyama, A., 2006. Terminal velocity of single drops in stagnant liquids. Journal of Fluid Science and Technology 1, 72–81.

Myint, Win, 2008. Drag and Lift Forces Acting on Single Drops. Ph.D. Thesis. Kobe University, Japan.

White, E.T., Beardmore, R.H., 1962. The velocity of rise of single cylindrical air bubbles through liquids contained in vertical tubes. Chemical Engineering Science 17, 351–361.

Xu, J.-J., Zhao, H.-K., 2003. An Eulerian formulation for solving partial differential equations along moving interface. Journal of Scientific Computing 19, 573–594.

Yamamoto, Y., Yamauchi, M., Uemura, T., 2008. Numerical simulation of a contaminated water drop sinking in a oil by a front-tracking method. Journal of Computational Science and Technology 2, 246–257.